Self-Consistent Integral Equation Theory of Polyolefins and Comparison to X-ray Scattering Experiments†

Jeffrey D. Weinhold* and John G. Curro

Sandia National Laboratories, Albuquerque, New Mexico 87185-1349

A. Habenschuss and J. D. Londono‡

Oak Ridge National Laboratory, Oak Ridge, Tennessee 37831

Received February 3, 1999; Revised Manuscript Received July 21, 1999

ABSTRACT: Self-consistent, polymer reference interaction site model (PRISM) calculations were performed on realistic models of three polyolefin melts: polyisobutylene (PIB), isotactic polypropylene (iPP), and syndiotactic polypropylene (sPP). In these calculations, both the *intra*molecular and *inter*molecular structure of the polymer liquid are determined in a self-consistent manner. The multiple-chain problem is mapped to an equivalent single-chain Monte Carlo simulation by representing the effect of the other chains through a "medium-induced" pairwise-additive potential calculated from PRISM theory. The intramolecular structure factor, intermolecular radial distribution functions, and medium-induced potentials are obtained numerically from a series of Monte Carlo simulations and PRISM calculations performed iteratively until a self-consistent solution is obtained. The resulting melt structure factors are in close agreement with X-ray scattering experiments on PIB at 25 °C and iPP and sPP liquids at 180 °C. The individual radial distribution functions between pairs of methyl, methylene, and methyne (or C atom in the case of PIB) on different macromolecules show universal behavior on long length scales; however, significant differences in local packing are found for distances less than about 12 Å. The resulting intramolecular structure functions can be employed as input to PRISM theory to deduce the packing and miscibility characteristics in polyolefin mixtures.

1. Introduction

Polyolefins are produced at lower cost and in larger volume than any other class of polymers. The monomers that comprise these polymers contain only carbon and hydrogen and are an abundant byproduct of petroleum refining. Despite their simple chemical composition, polyolefins exhibit a wide range of useful mechanical properties due to varying degrees of branching and crystallinity. The study of polyolefin structure in the melt state provides a fundamental understanding of how the size of side groups and their spacing along the polymer backbone affects the molecules' ability to pack closely together. For example, the repeating methyl side groups in polyisobutylene allow for efficient packing of the chains,[1] and the resulting high density appears to be one reason for the excellent gas barrier properties that butyl rubber exhibits.

Simulations of many-chain systems are one way to explore the effect of polyolefin architecture on packing structure. These simulations[2−4] have used realistic models in which the polymers are composed of overlapping spheres where each of these interaction sites represents either a particular atom (C or H) or a small grouping of atoms (CH_2, CH_3, etc.). Unfortunately, these studies have several restrictions caused by the limited capability of even the fastest computers available today. The first restriction is the system size. For the most efficient algorithm, the time required by the simulation increases at least in proportion to the number of sites in the system. Studies of bulk systems can reduce the total number of sites somewhat by using periodic boundary conditions. However, periodic boundaries cannot be used as freely with polymers as with small molecule systems since a single molecule should not be allowed to stretch through two opposing sides of the simulation box and interact with a periodic image of itself. Therefore, the width of the simulation box must increase in proportion to the end-to-end distance which depends on chain length, N, through the relation $\langle R^2 \rangle^{0.5} \propto \sqrt{N}$. To maintain a constant density with this change of box size, the number of molecules must also increase in proportion to $N^{0.5}$. The combination of more molecules and more segments per molecule causes the amount of computer time necessary for the simulation to increase very rapidly with N. Therefore, polymer simulations are usually restricted to relatively low molecular weight systems.

The use of realistic polymer models complicates the simulation of many-chain systems even further. Whereas simulations of coarse-grained models can use an abundance of efficient Monte Carlo (MC) motions such as crankshaft and reptation,[5] atomistic models at liquidlike densities are generally simulated through molecular dynamics (MD) techniques because of the low probability of acceptance of standard MC moves. While the relaxation and diffusion of a coarse-grained polymer model in a MD simulation normally requires a large amount of computer time,[6] the tight packing exhibited by an atomistic model of polyisobutylene will make this problem even worse. Therefore, many-chain simulations of realistic models may not sample a wide variety of configurational states within a reasonable amount of computer time.[6]

† Work at Sandia National Laboratories supported by the U.S. Department of Energy under Contract DE-AC04-94AL85000. Work at Oak Ridge National Laboratory supported by the U.S. Department of Energy under Contract DE-AC05-96OR22464.

‡ Present address: E.I. Dupont Experimental Station Laboratory, Wilmington, DE 19880.

* Corresponding author.

10.1021/ma990150y CCC: $18.00
Published on Web 09/21/1999

An alternative to simulations of many-chain systems is provided by the polymer reference interaction site model or PRISM theory.[7−10] This theory takes as input the structure of a single molecule, the interactions between molecules, and the system density. With this information the theory is able to determine the structure of the many-chain system. Tests using coarse-grained models have shown the PRISM predictions to be in close agreement with the structure determined by many-chain simulations.[11,12] For PRISM studies using models more complex than a semiflexible (Koyama) chain,[13] a simulation must be performed to calculate the single molecule intramolecular structure. Once this structure has been determined, the PRISM equations can be solved in a small amount of computer time. Therefore, most of the computational effort is focused on the simulation of a single molecule, and compared to a many-chain simulation, this calculation will require considerably less computer time because of the greatly reduced number of sites. In addition, performing a simulation on only a single molecule allows large conformational changes to occur that would ordinarily create many high-energy overlaps when other molecules are present. Therefore, Monte Carlo techniques are possible even for atomistic models since MC moves such as pivot[14] now have a reasonable probability of acceptance. By reducing the many-chain problem to that of a single chain, PRISM allows the structure of atomistic models at long chain lengths to be determined in a computationally efficient manner.

Since the properties of the many-chain system determined by PRISM are highly dependent on the single-chain structure, it is critical that the single-molecule simulation generate a structure representative of a polymer in the melt. If a simulation is performed with only Lennard-Jones interactions between all segments, the repulsions between segments usually results in a structure that is more characteristic of a chain in a good solvent than in a melt. Therefore, most studies using PRISM have assumed the Flory ideality hypothesis[15] that at meltlike densities the excluded volume of segments is screened. A single-chain simulation would then include local structural details (bond angles, torsional potentials, and short-range dispersive interactions) but no interactions between segments separated by more than a certain (∼5) number of bonds.[16] Although this approach gives the correct scaling for polymer dimensions in the melt ($\langle R^2 \rangle \propto N$), there are two disadvantages to assuming ideality. First, the absence of repulsions between segments separated by several bonds allows the simulation to generate structures having a number of overlapping segments. Whenever these overlaps occur, the polymer occupies less volume than a true melt conformation. To achieve the same fraction of occupied volume as in experiment, the density that is used in PRISM must now be higher than the experimental value. Previous studies[12,16,17] have attempted to quantify the amount of overlap using the simplifying assumption that all overlap involves only two sites. Since a significant fraction of the overlapping volume in an atomistic model is shared by three or more sites, the "corrected" density that comes out of this procedure actually corresponds to an upper bound. An alternative approach, in which the density is adjusted to match the PRISM zero wavevector structure factor to experimental compressibility data,[16] reduces the predictive capability of these studies. The uncertainty in the value of density necessary to correct for the assumption of ideality of the single chain represents a limitation to these calculations.

A second disadvantage to assuming ideality is that the form and strength of the potentials to be used in the single-chain simulation are no longer obvious. The characteristic ratio is sensitive not only to the strength and magnitude of the site/site potentials but also to the cutoff distance along the chain backbone beyond which excluded-volume interactions become screened. As a result, the potential parameters are generally not transferrable from one polymer to another. The ability to predict properties of materials not yet synthesized would be greatly enhanced if the single-molecule simulation used the same potentials as have been found to be optimal for many-chain simulations.

An approach that avoids the disadvantages of assuming ideality is self-consistent PRISM theory.[7] In this technique excluded volume is no longer assumed to be screened, and the single molecule simulation is performed with repulsive interactions between all segments. While this first single-chain structure is unlikely to be representative of the melt, PRISM theory can determine the effective solvation potential exerted on the single chain by the other molecules. Another single-chain simulation is then performed, but this time the interactions between all segments are described by the sum of the solvation and the repulsive potential. The results of this simulation are used to generate the next solvation potential, and this procedure is repeated until neither the simulated structure nor the solvation potential changes significantly from one iteration to the next. This self-consistent single-chain structure will not contain any of the unphysical site overlaps that result from assuming ideality, and therefore, the experimentally known density should be used in PRISM theory. In addition, the strength of the solvation potential controls the tendency toward compact or expanded polymer conformations, and since the Lennard-Jones parameters no longer need to be adjusted to match the characteristic ratio to experiment, standard values for these dispersive interactions may be used.

The framework for self-consistent studies within RISM theory[18,19] was first developed by Chandler and Pratt,[20] and this technique has been applied to alkane fluids.[21] These calculations have been extended to linear polymer models through optimized perturbation,[22,23] variational free energy,[24,25] and Monte Carlo[25,26] procedures. The most complex form of the variational approach[25] shows good agreement with many-chain simulations over a range of densities although the predicted polymer conformation size is too small. When the single-chain structure is determined by a Monte Carlo simulation,[25,26] good agreement is also obtained but with larger polymer sizes than is seen in many-chain simulations. The self-consistent procedure has also been applied to star polymers[27] and block copolymers[28] while studies of polymer solutions[29] and blends[30] have shown good agreement with many-molecule simulations of these mixtures.

This paper reports the first application of self-consistent PRISM theory to atomistic polymer models. The polyolefins polyisobutylene and isotactic and syndiotactic polypropylene have been studied using united atom models, and their structure has been compared to that from X-ray scattering experiments. The remainder of this paper begins with a description of PRISM

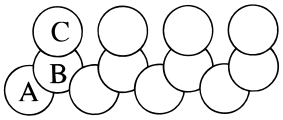

Polypropylene

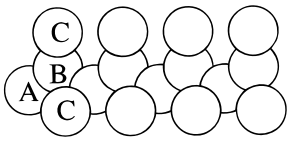

Polyisobutylene

Figure 1. Schematic representation of the united atom model for polyisobutylene and polypropylene. Sites A and C refer to the CH_2 and CH_3 groups while the B site corresponds to a carbon atom in PIB and a CH group in polypropylene.

theory and details about the self-consistent calculation of structure. The following section will describe the single-chain Monte Carlo simulation procedure which is necessary due to the complexity of the polymer model. Then the results will be presented and discussed along with comparisons to X-ray scattering experiments. The final section will then provide conclusions.

2. PRISM Theory

PRISM is the extension to polymers of the reference interaction site model (RISM) of Chandler and Andersen.[18,19] A thorough review of polymer RISM theory has been provided in ref 7. The work presented in this paper differs from most of the previous studies in two respects: (1) the self-consistent solution of intra- and intermolecular structure and (2) the use of a united atom model with a multiple number of sites. Figure 1 depicts how polypropylene and polyisobutylene are modeled. In a united atom model, each carbon atom and all hydrogens bonded to it are represented as a single sphere which overlaps with its bonded neighbors. For clarity, we designate the different sites as A, B, and C where A and C correspond to the CH_2 and CH_3 groups, respectively, and B is the branch site on both polymers. Note that the B site is a CH moiety in polypropylene and a bare C in polyisobutylene, and therefore, the B sites have slightly different potentials in the two polymers.

2.1. Multiple Site Formalism. PRISM has been generalized for multiple site polymers in previous work.[31] The main goal of PRISM is to determine the intermolecular packing through a matrix of radial distribution functions:

$$\tilde{\rho}^2 g_{\alpha\gamma}(r) = \langle \sum_{i\neq j=1}^{N_c} \delta(\vec{r}_i^{\,\alpha})\, \delta(\vec{r} - \vec{r}_j^{\,\gamma}) \rangle \qquad (1)$$

where N_c is the number of chains, $\tilde{\rho} = N_c/V$ is the chain density, and $\vec{r}_i^{\,\alpha}$ is the position vector of site α on chain i. By neglecting end effects,[7] all monomers along the chain backbone become equivalent, and the indices α and γ in eq 1 correspond to one of the three types of sites A, B, or C.

Since the polyolefins studied in this paper each have three distinct sites, the set of integral equations can be written using 3×3 matrices for each of the variables. The key relationship between intra- and intermolecular structure is provided by the generalized Ornstein−Zernike equation of Chandler and Andersen.[18,19] This equation can be shown in Fourier Transform space as

$$\hat{\mathbf{h}}(k) = \hat{\mathbf{\Omega}}(k)\cdot\hat{\mathbf{C}}(k)\cdot[\hat{\mathbf{\Omega}}^{\mathrm{T}}(k) + \boldsymbol{\rho}\cdot\hat{\mathbf{h}}(k)] \qquad (2)$$

where the caret denotes Fourier transformation with wave vector k. Here $\boldsymbol{\rho}$ is a diagonal matrix of the site densities, and $\hat{\mathbf{h}}(k)$ is the matrix of intermolecular pair correlation functions, $h_{mm'}(r) = g_{mm'}(r) - 1$, after transformation. The matrix $\hat{\mathbf{\Omega}}(k)$ contains the intramolecular pair correlations. All of the information about chain architecture, which is the only factor distinguishing isotactic and syndiotactic polypropylene, is contained within $\hat{\mathbf{\Omega}}(k)$. The individual elements of this matrix can be determined through

$$\hat{\Omega}_{\alpha\gamma}(k) = \frac{1}{N_\alpha}\sum_{i\in\alpha}\sum_{j\in\gamma}\left\langle \frac{\sin kr_{ij}}{kr_{ij}} \right\rangle \qquad (3)$$

where N_α is the number of sites of type α in the polymer.

When using the generalized Ornstein−Zernike equation, $\hat{\mathbf{\Omega}}(k)$ is known and $\hat{\mathbf{h}}(k)$ is the variable to be determined. The final variable that appears in eq 2 is the direct correlation function matrix, $\hat{\mathbf{C}}(k)$. Since this function is also unknown, an approximation must be introduced in order to solve eq 2. As in the case of atomic liquids,[32] the structure of polymer liquids at high density is determined almost entirely by the repulsive branch of the potential, provided the attractive part of the potential is weak which is the case for van der Waals interactions. For the purpose of calculating the packing in polyolefin melts, we use only the repulsive part of the potentials and employ the atomic Percus−Yevick closure:[7,32]

$$C_{mm'}(r) = \{1 - \exp[\beta v_{mm'}(r)]\} g_{mm'}(r) \qquad (4)$$

where $v_{mm'}(r)$ is the repulsive potential between sites of type m and m' and $\beta = 1/k_B T$. To remain consistent with the Monte Carlo single-chain simulation (see section III), $v_{mm'}(r)$ had the form of a Lennard-Jones 6−12 potential with a cutoff at $r = \sigma$. Therefore, only the repulsive part of the potential was used. Since the exact direct correlation function for a dense liquid approaches 0 quickly at $r > \sigma$,[32] the approximation introduced by eq 4, primarily $C_{mm'}(r) = 0$ at all $r > \sigma$, is fairly accurate. After applying this closure, the set of coupled integral equations can then be solved by Picard iteration techniques.[31] We note that attractive interactions are important in the computation of thermodynamic properties and can be included from standard perturbation theory[32] using the $g_{mm'}(r)$ correlation functions obtained from the repulsive reference system.

2.2. Self-Consistent Determination of Structure. The intermolecular structure of a polymer melt is highly dependent on the average intramolecular structure of the individual polymers. For example, collapsed polymers would show a very deep but short-range correlation hole in $g_{mm'}(r)$. In contrast, expanded polymer conformations have a much shallower correlation hole, and therefore, these polymers tend to have many more contacts with other chains than a collapsed polymer. At the same time, intermolecular interactions affect the structure of a single molecule. For example, polymers at low concentration in good solvent will be swollen, but as the polymer concentration increases, the larger number of repulsions between polymers causes the

Table 1. Density and Lennard-Jones Parameters[a]

polymer	ρ	σ_{AA}	ϵ_{AA}	σ_{BB}	ϵ_{BB}	σ_{CC}	ϵ_{CC}	$\sigma_{AC}{}^{15}$	$\sigma_{CC}{}^{15}$	$\sigma_{AB}{}^{14}$	$\sigma_{BC}{}^{14}$
PIB	0.009 80	3.93	94	3.80	50	3.93	156	3.725	3.531	*b*	*b*
iPP	0.010 94	3.93	94	3.85	64	3.93	156	3.40	3.40	3.20	3.20
sPP	0.010 94	3.93	94	3.85	64	3.93	156	3.50	3.00	3.50	3.00

[a] Units are as follows: ρ, monomers Å^{-3}; σ, Å; ϵ, cal mol^{-1}. [b] Values of σ for 1−4 pairs in PIB were identical to those used for 1−6 and longer range pairs. Instead, the magnitude of the potential ($\epsilon_{\alpha\gamma}{}^{14}$) was reduced by a factor of 2.

chain conformations to contract and eventually approach melt dimensions.[15,33,34] The true conformation of a polymer in the melt arises from a balance (self-consistency) between intra- and intermolecular effects.

A self-consistent solution must be obtained through an iterative procedure since $\hat{\mathbf{\Omega}}(k)$ must be treated as a known quantity in order to solve eq 2 for $\hat{\mathbf{h}}(k)$. Whereas the single-chain simulation interfaces with PRISM by providing $\hat{\mathbf{\Omega}}(k)$, PRISM influences the next simulation through an effective solvation potential. The total potential energy in the simulation is[22]

$$U(\tilde{R}) = U_0 + U_E + W(\tilde{R}) \tag{5}$$

where $\tilde{R}$ represents the set of coordinates necessary to define an instantaneous polymer conformation and U_0 contains all of the bonded constraints (bond bending, torsional energies). U_E is the sum over all repulsive interactions that prevent overlap between two segments of the same molecule, and since a long-range nonbonded interaction between two segments of the same chain should be equivalent to the interaction between segments on different chains, U_E should be a sum over the same potential as is used in the closure relation, eq 4. $W(\tilde{R})$ is the solvation energy which quantifies the effect of the other molecules on the single chain. In general, U_E causes the conformation to expand while $W(\tilde{R})$ will cause it to contract in order to pack more efficiently with other molecules. The essence of the Flory ideality hypothesis[15] is that the effects of U_E and $W(\tilde{R})$ cancel each other.

To begin the self-consistent iteration procedure, a first guess for $\hat{\mathbf{\Omega}}(k)$ must be generated. A suitable guess can be determined through a single-chain simulation with $W(\tilde{R}) = 0$, and this simulation will tend to give a swollen polymer conformation. From the solution to eq 2 we also obtain the direct correlation function matrix, $\hat{\mathbf{C}}(k)$, and the static structure factor

$$\hat{S}_{mm'}(k) = \rho_m \hat{\Omega}_{mm'}(k) + \rho_m \rho_{m'} \hat{h}_{mm'}(k) \tag{6}$$

These are the two quantities necessary to calculate the solvation potential matrix, $\hat{\mathbf{W}}(k)$. Although the solvation potential should be considered to be an N-body potential where N is the number of sites, here we follow previous work and assume the potential to be pairwise decomposable. Therefore, the potential is added to the short-range Lennard-Jones repulsions to define the interaction between sites in the next single-chain simulation. Two forms have been proposed for the solvation potential,[35,36] and after generalizing to a multisite polymer,[27,28] the formulas can be written as

$$\beta\hat{\mathbf{W}}(k) = -\hat{\mathbf{C}}\hat{\mathbf{S}}\hat{\mathbf{C}} \tag{7a}$$

$$\beta\hat{\mathbf{W}}(k) = -\ln[1 + \hat{\mathbf{C}}\hat{\mathbf{S}}\hat{\mathbf{C}}] \tag{7b}$$

Equation 7a was proposed by Chandler et al. [35] and is denoted here as the CSR solvation potential. An alternative form, the GS solvation potential shown in eq 7b, was derived by Grayce and Schweizer by making similar assumptions to those used in the Percus−Yevick closure.[36]

Table 2. Bond Angle Potential Parameters[a]

polymer	param	ABA	BAB	ABC	CBC
PIB	k_θ	105	70	70	70
	θ_0	112	112	107.8	107.8
iPP/sPP	k_θ	105	70	70	70
	θ_0	111	114	108.8	106.5

[a] Units are as follows: k_θ, cal deg^{-2} mol^{-1}; θ_0, deg.

The solvation potential is an oscillating function with both attractive and repulsive regions. Unlike the Lennard-Jones repulsions, the solvation potential is not expected to be short range. Instead, the use of $W_{mm'}(r)$ in the next single-chain simulation should alter the conformations in a manner that allows the molecules to pack together more efficiently. If the first guess for $\hat{\mathbf{\Omega}}(k)$ is a swollen conformation, the resulting $\hat{\mathbf{W}}(k)$ will likely favor more collapsed polymers. After several more iterations, a balance eventually forms between the intra- and intermolecular effects, and a self-consistent solution is obtained.

3. Simulation Procedure

Earlier PRISM studies demonstrated that structure factors determined from a united atom model matched X-ray scattering experiments as closely as an explicit atom model.[16] Since united atoms also require less computational time, we have chosen to use this model. Therefore, the simulated polymers consisted of overlapping spheres with Lennard-Jones σ values ranging from 3.8 to 3.93 Å (see Table 1), and bonded spheres were held at a fixed bond length of 1.54 Å. Chain lengths of 50 and 200 monomers were studied. Unlike our previous work on polypropylene,[16] the bond angles were not held fixed in these simulations. Instead, varying bond angles were employed to allow for cooperativity between dihedral angle rotation and bond angle vibrations present in real polyolefin chains. The bond angle potential had the form

$$V_\theta = \frac{k_\theta}{2}(\theta - \theta_0)^2 \tag{8}$$

Values for k_θ and θ_0 are given in Table 2.

For a truly self-consistent solution between PRISM and single-chain simulation, the same nonbonded interactions should be used in both techniques. Since the structure of systems at liquidlike densities is almost exclusively determined by repulsive interactions and the absence of attractions allows PRISM to use the simpler atomic closures, we have used only repulsive interactions in U_E (eq 5) and $v_{mm'}(r)$ (eq 4). A Lennard-Jones

6−12 potential was used:

$$v_{mm'}(r) = 4\epsilon_{mm'}\left[\left(\frac{\sigma_{mm'}}{r}\right)^{12} - \left(\frac{\sigma_{mm'}}{r}\right)^{6}\right] \quad r < \sigma_{mm'}$$

$$v_{mm'}(r) = 0 \quad r \geq \sigma_{mm'} \tag{9}$$

with a cutoff at $r = \sigma_{mm'}$. The values of ϵ_{mm} and σ_{mm} for CH_3, CH_2, and CH were taken from the united atom potentials of Siepmann et al.[37] The parameters for the bare carbon in polyisobutylene (the B site) were those suggested by Jorgensen et al.[38] Table 1 summarizes the parameters that were used. Following the suggestions of both papers,[37,38] Bertholet scaling was assumed for both the well depth, $\epsilon_{mm'} = \sqrt{\epsilon_{mm}\epsilon_{m'm'}}$, and the site diameter, $\sigma_{mm'} = \sqrt{\sigma_{mm}\sigma_{m'm'}}$. The full potential was used for all sites separated by five or more bonds, and no Lennard-Jones potential was used for sites separated by one or two bonds. In a polyolefin like polyisobutylene, the backbone bond angles are large in order to reduce steric repulsions. To couple this change in bond angle to torsional energies, Lennard-Jones potentials were also used between sites separated by three bonds. Since the standard Lennard-Jones parameters tend to overpredict the repulsion between sites separated by a few bonds, the strength of this three-bond potential in polyisobutylene was reduced by a factor of 2. For both stereoisomers of polypropylene, smaller values of the Lennard-Jones σ parameter (σ_{14} in Table 1) were used to reduce the magnitude of the three-bond repulsion. The remainder of the interaction energy between sites separated by three bonds was accounted for through a rotational potential as described later in this section.

One limitation of a united atom model is its inability to account for the interlocking of hydrogens.[39] For example, at low temperatures one would expect that two methane molecules would be able to come close together by having their hydrogen atoms mesh together. For small molecules at experimental temperatures this effect is usually unimportant since the interacting sites are on different molecules and are moving too fast relative to each other for interlocking to be significant. However, the constraints between two sites that are on the same molecule and separated by only a few bonds will generally force the sites to move in a similar manner. In each of the polymers studied here, the 1−5 interactions (i.e., between sites separated by four bonds) either involve two C sites or a C and an A. Since the methyl side groups (C sites) are somewhat free to rotate, we expect that these 1−5 pairs are able to approach closer than is possible whenever Lennard-Jones parameters optimized for intermolecular interactions are used. As was seen in our previous work with polypropylene,[16] the use of a smaller value of σ for these 1−5 interactions has a dramatic effect on the characteristic ratio and structure factor. Table 1 gives the values of σ_{15} used in the simulations. In all of the Lennard-Jones interactions (1−4 pairs and higher) the standard Siepmann[37] or Jorgensen[38] values of ϵ are used, and we assume that 1−6 and higher pair interactions have enough independent motion such that interlocking is no longer significant.

The Lennard-Jones potential between sites separated by three bonds provides one component of the torsional energy. Since a united atom model is used rather than explicit atoms, another potential is necessary to account for the contribution of the hydrogen atoms on the backbone carbons to the torsional energy. This effect was provided through the potentials:

$$V_\phi = \frac{1}{2}k_\phi\left[1 - \frac{\cos[3\phi] - \cos[3(\phi+\gamma)] - \cos[3(\phi-\gamma)]}{3}\right] \tag{10a}$$

$$V_\phi = \frac{1}{2}k_\phi\left[1 - \frac{2\cos[3\phi] - \cos[3(\phi\pm\gamma)]}{3}\right] \tag{10b}$$

$$\gamma = \sin^{-1}\left(\frac{\sin(\beta)}{\sin(\theta)}\right)$$

where ϕ is the backbone rotational angle, β is the angle of a C site with respect to the plane formed by the nearest two backbone bonds, and θ is the A−B−C bond angle. The angle γ describes the location of the C sites after they are projected onto the plane perpendicular to the corresponding A−B bond. The constant k_ϕ was set to 2900 cal/mol for each of the polymers. Equation 10a was used in the simulations of polyisobutylene. Isotactic and syndiotactic polypropylene used eq 10b where the sign in the second cosine term switches between + and − as a result of the tacticity.

The simulations were performed with two types of Monte Carlo moves. Large conformational changes were made by pivot moves[14] in which one of the backbone bonds was chosen randomly and a new value of rotational angle, ϕ, for this bond was chosen. In conjunction with this pivot motion, the bond angle formed by the selected bond and the neighboring bond closest to a chain end was increased or decreased by a random amount. An acceptance ratio of 4−5% was typical for this move. The second Monte Carlo move involved randomly selecting one of the monomers and changing the angle β formed by the B−C bond and the plane formed by the two neighboring backbone bonds. In polyisobutylene, both C sites on a monomer were characterized by a single value of β. For each of the polyolefins the C sites were moved such that the bond angles with the two A sites are equal. Both Monte Carlo moves were accepted or rejected using Metropolis importance sampling.[40] To match the experimental data, the studies of polyisobutylene were performed at 25 °C while both forms of polypropylene were modeled at 180 °C.

The final item listed in Table 1 is the polymer melt density known from experiment. These values were derived from equations of state for PIB[41] and isotactic polypropylene.[42] Since an accurate equation of state for sPP was unavailable, it was assumed to be equivalent to iPP. These densities enter the self-consistent procedure during the PRISM step through eqs 2 and 6.

For most cases the self-consistent calculation was run for 20−30 iterations. The number of attempted Monte Carlo moves increased with the number of iterations, and the final iterations typically consisted of 4×10^6 (3×10^7) attempted pivot moves for chains of 50 (200) monomers.

4. Results and Discussion

4.1. Solvation Potentials and Self-Consistency.

To obtain a self-consistent solution between single-chain simulation and PRISM theory, each technique must have a way to influence the other. PRISM is able to alter the single-chain structure by providing a solvation potential, $W_{mm'}(r)$, to be used in the simulation. Figure

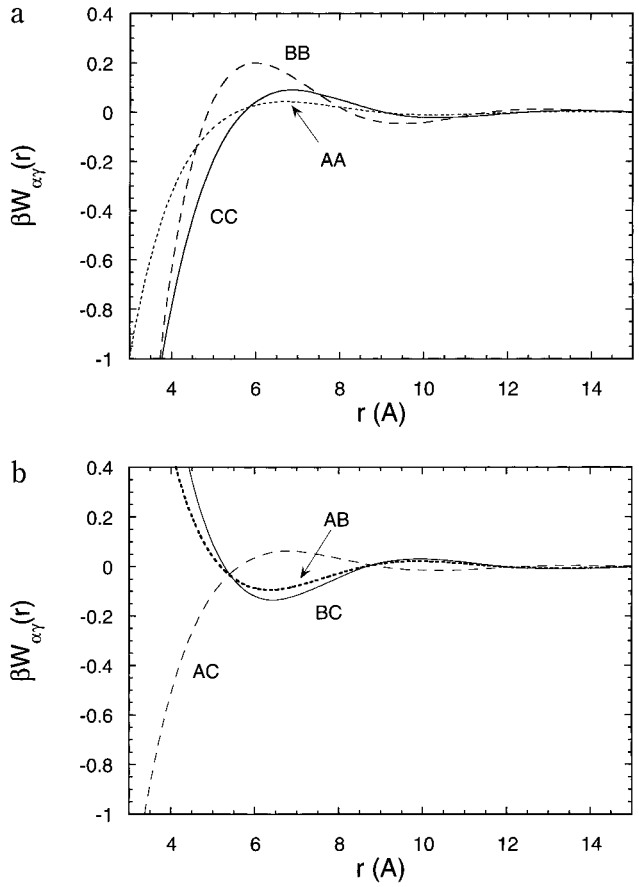

Figure 2. Solvation potentials for PIB as a function of r: (a) correlations between site of the same type; (b) correlations between unlike pairs of sites. These values were determined from the CSR form (eq 7a) of the solvation potential.

2 presents the final $W_{mm'}(r)$ determined for polyisobutylene from eq 7a, the CSR form of the solvation potential. Since PIB has three distinct sites (the two methyls are equivalent), there are six different pairs and, therefore, six different solvation potentials. The pairs AA, BB, CC, and AC show the most important features of the potential. At short distances, $W_{mm'}(r)$ for these pairs is attractive which is necessary to counteract the tendency for this nonoverlapping chain to have conformation sizes typical of a polymer in good solvent. The attractive portion of the solvation potential instead mimics the many unfavorable repulsions that a chain would experience if it were to expand while surrounded by a meltlike density of other molecules. The second important feature of the solvation potentials is that they oscillate about zero at intermediate and high distances. These attractive and repulsive regions of the potential tend to align the segments of the chain into evenly spaced coordination shells. Forcing the sites to arrange in this manner improves the single chain's ability to pack tightly with many other molecules.

Solvation potentials for the pairs AB and BC show a different trend than the other pairs. In Figure 2 $W_{mm'}(r)$ for these two pairs appears as an inverted image of the other pairs, being repulsive at short distances and showing maxima where the others show minima and vice versa. This difference is likely due to the B site having several sites bonded to it which prevent the B site from coming close to other polymer segments. The inability of the B site to approach other sites will cause the short-range repulsive part of the solvation potential to have little effect. The oscillations in $W_{mm'}(r)$ at higher

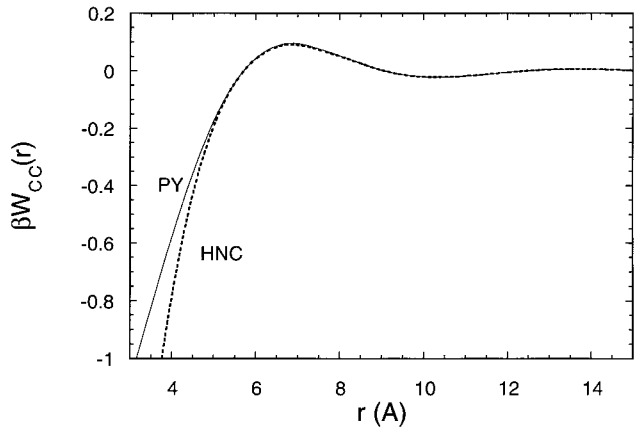

Figure 3. Comparison of the solvation potential between C sites for PIB using the HNC-like CSR (eq 7a) and Percus–Vevick style GS (eq 7b) forms.

r will affect the structure, but the overall interaction between two monomers will likely be more representative of the potentials not involving a B site because of the greater number of these pairs. The solvation potentials for polypropylene show the same trends as in PIB, but the magnitude of the short-range attractions and repulsions is smaller. This trend is consistent with the idea that the different behavior of the solvation potentials arises from a site that is shielded from nonbonded contacts, and the magnitude of the disparity will depend on the degree of the shielding.

An interesting note is that the different trends involving the B site are not equivalent to the "ghost site" problems observed in RISM studies.[43] In those cases, the intermolecular structure was altered by the addition of a noninteracting site that is completely shielded by other intramolecular sites. For polyisobutylene the intermolecular structure does change as the size of the B site shrinks. However, the structure obtained from PRISM with a B site of infinitesimal size is identical to that found by treating PIB as a collection of only A and C sites.

An important consideration for self-consistent PRISM studies is the form of the solvation potential to use. Figure 3 compares the CSR (eq 7a) and GS (eq 7b) forms of the solvation potential between methyl sites on PIB. Since these are the most exposed sites on the polymer, $W_{CC}(r)$ will have the strongest effect on the single-chain structure. The figure shows that the CSR solvation potential has much stronger short-range attractions than the GS form. However, the two solvation potentials are virtually identical at distances ($r > 5$ Å) beyond this short-range attractive region. Previous studies[25] have compared the solvation potentials for melts of fully flexible tangent-sphere chains using Monte Carlo single-chain simulations to determine ω. The self-consistent solutions for both solvation potentials typically predicted conformation sizes that were larger than seen in many-chain simulations at low to moderate densities. Since the stronger short-range attractions of the CSR potential resulted in smaller conformation sizes, the CSR form appeared to be in slightly better agreement with simulation over the limited range of densities. However, at meltlike densities the CSR potential showed a dramatic collapse of the freely jointed chain polymers. Since this behavior has not been observed in either experiment or simulation, the authors concluded that the GS solvation potential is more appropriate for polymers at meltlike densities.[25] Yethiraj[44] has sug-

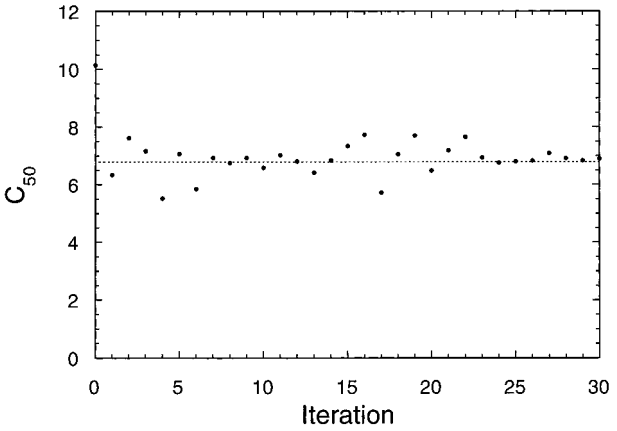

Figure 4. Characteristic ratio, C_{50}, as a function of the number of iterations for a 50-mer of PIB. The data point at iteration = 0 is the first guess in which no solvation potential was used. The dashed line is the value determined through experiments on high molecular weight PIB.

gested instead that the correct conformation sizes are obtained when the assumptions used to derive the solvation potential match those of the closure used in PRISM. Therefore, the collapse observed in earlier studies was the result of using the PY closure with the HNC-like CSR solvation potential.

Solutions to the PRISM equations for the structure of polyolefins were also made by using the HNC closure

$$C_{mm'}(r) = -\beta v_{mm'}(r) + g(r) - 1 - \log[g(r)] \quad (11)$$

in place of the PY closure (eq 4). For these polyolefins convergence is more difficult to obtain with the HNC closure, and a greatly increased number of Picard iterations are required. In addition, the structure factor shows unphysically high values at low wavevector similar to that observed by Yethiraj and Schweizer.[23] For these two reasons, the PY closure was employed for all of the presented results.

Figure 4 presents the dependence of the conformation size on the number of iterations for a 50-monomer isobutylene chain using the CSR solvation potential. The conformation size is reported as the characteristic ratio $C_N = \langle R^2 \rangle / N_b l^2$ where $\langle R^2 \rangle$ is the mean-squared end-to-end distance, N_b is the number of bonds, and l is the bond length. The high characteristic ratio $C_{50} = 10.2$ at iteration zero is the result of the first guess of the single-chain structure in which the simulation used repulsive interactions between all sites but no solvation potential. The first several iterations have a tendency to alternate between high and low values of the conformation size. After 22 iterations the variation from one iteration to the next becomes very small, and the final iterations converge to a characteristic ratio of 6.9. Repeating the calculation with the GS solvation potential shows similar behavior and converges to $C_{50} = 7.1$. The agreement between these predictions and the value of 6.8 obtained from neutron scattering experiments[45] is somewhat fortuitous since, once the chain length is increased to 200 monomers, a characteristic ratio of 8.5 is obtained. To match the characteristic ratio of this higher molecular weight to the experimental value, the strengths of the solvation potentials were increased by multiplying by a factor greater than 1. For a 200-mer of polyisobutylene, a factor of 1.092 was necessary to obtain a self-consistent solution with $C_{200} = 6.8$. This factor is necessary because the solvation potentials are approximate. This is primarily the result of assuming the potential to be pairwise-decomposable in order to achieve a mathematically tractible form. Recent work by Grayce[46] has instead shown that many-body interactions provide a significant contribution to the overall solvation energy. Although the need for an adjustment factor reduces the ability to predict the properties of polymers with unknown characteristic ratios, the development of other forms of the solvation potential is beyond the scope of this paper. An interesting note is that the total pair correlation function $S(r)$ is virtually insensitive to the characteristic ratio. Therefore, changes in the size of the single chain are counteracted by equivalent changes in the correlation hole region of $g(r)$. This behavior suggests that properties such as the X-ray scattering structure factor can be predicted without knowledge of the characteristic ratio. However, since mixing properties are highly dependent on the number of intermolecular contacts, blend miscibility is expected to be sensitive to the characteristic ratio. Since scattering experiments do not provide a sensitive test of the theory's ability to predict chain dimensions, full many-chain simulations are currently being performed to compare to these predictions.

4.2. Intramolecular Structure. The structure of a single polymer chain is the key input to PRISM theory, and the goal of the self-consistent procedure is to determine this structure in a manner that balances the higher single-chain entropy with the increased number of intermolecular repulsions that would result from an expanded conformation. In Fourier transform space, the main trends in $\omega(k)$ are best viewed in three distinct wavevector regimes. First at low values of $k \ll 1/R_g$, the structure has a direct dependence on the radius of gyration of the chain. In the intermediate scaling regime, $1/R_g < k < 1/\sigma$, $\omega(k)$ is closely related to the statistical segment length of the polymer, σ and is thought to be generally chain length independent. Finally, at values of k well above $1/\sigma$ short-range intramolecular correlations dominate the structure factor, and this region should be equivalent for all molecular weights of the same polymer. Understanding the dependence of $\omega(k)$ on chain length creates the possibility of extrapolating the structure to very high molecular weights for PRISM studies. Therefore, we have examined each of these regions of wavevector in detail.

In the limit of zero wavevector, the scattering of a single molecule is a function of its radius of gyration. Following the ideas of Guinier,[47] the low wavevector scattering can be studied through

$$\frac{\hat{\omega}_{\alpha\gamma}(0)}{\hat{\omega}_{\alpha\gamma}(k)} = 1 + \frac{1}{3}k^2 R_g^2 + O(k^4) \quad (12)$$

where $\omega_{\alpha\gamma}(0)$ is the number of sites of type α in the molecule. When k is small, all terms of higher order than k^2 can be ignored. Therefore, a plot of $\hat{\omega}_{\alpha\gamma}(0)/\hat{\omega}_{\alpha\gamma}(k)$ vs k^2 should yield a slope that is proportional to R_g^2. Figure 5 shows this Ornstein−Zernike plot for ω_{cc} of PIB at chain lengths of 50 and 200 monomers. The slope of the data for $N = 200$ is much larger than for the shorter chains, and using the first data points to determine the slope suggests that R_g^2 is 261 and 1098 Å^2 for chains of 50 and 200 monomers, respectively. These numbers match closely to the values 272 ($N = 50$) and 1062 ($N = 200$) that are expected on the basis of the simulations' characteristic ratios. The same slope

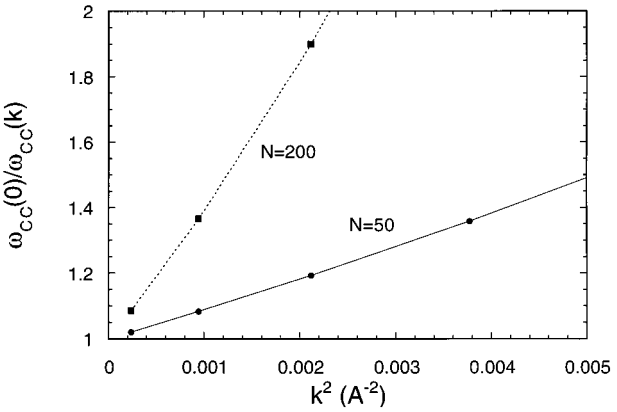

Figure 5. Ornstein−Zernike plot for the low wavevector intramolecular structure factor of C sites in polyisobutylene. The squares correspond to a 200-mer of PIB while the circles are for $N = 50$.

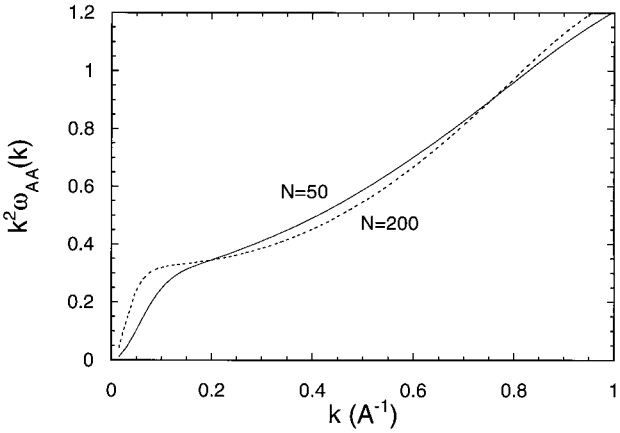

Figure 6. Kratky plot of the intermediate wavevector intramolecular structure between A sites of polyisobutylene. The solid and dashed lines correspond to PIB molecules of length 50 and 200, respectively.

is observed for the other combinations of sites as well. This Ornstein−Zernike analysis appears to be very appropriate for these molecules.

As the wavevector increases beyond $1/R_g$, the intermediate scaling regime begins. Kratky plots, $k^2\hat{\omega}_{\alpha\gamma}(k)$ vs k, have been particularly useful for evaluating experimental data in this region. For high polymers these plots have shown a plateau region which is the result of the intramolecular correlations following Gaussian statistics. By making a Lorentzian approximation to the Gaussian model, $\hat{\omega}_{\alpha\gamma}(k)$ can be described by[48]

$$\hat{\omega}_{\alpha\gamma}(k) = \frac{1}{k^2\sigma^2/12 + N^{-1}} \qquad (13)$$

where σ is the statistical segment length. Thus, the height of the plateau allows σ to be determined. Figure 6 presents this plot for the AA correlations in PIB. The depicted trend is very similar to that observed for rotational isomeric state studies of polyethylene.[49] The beginning of this scaling regime is marked by a hint of a plateau region followed by an inflection point. However, the slope then increases, and no true plateau is observed. Therefore, no single value of the statistical segment length can be assigned. In the studies of polyethylene the lack of a plateau was attributed to the chain lengths being too short to attain Gaussian statistics.[49] The comparison between the data for $N = 200$ and $N = 50$ in Figure 6 supports this idea since the higher initial slope for the longer chains causes the intermediate scaling regime to begin at lower wavevector and show indications of a plateau. Figure 7 depicts the corresponding plot for the CC correlations in PIB. Unlike the plot for $\hat{\omega}_{AA}(k)$, the CC structure shows a plateau even for 50 monomer chains. The data for the two chain lengths indicate that the longer chains have a wider and flatter plateau and a slightly larger value of the statistical segment length. Using the height of the plateau for $N = 200$ with eq 13 defines a statistical segment length of approximately 6.3 Å. On the basis of this equation, the plateau for the shorter chains would be expected to be slightly (<2%) lower if the values of σ are equivalent. There are two possible reasons for the disagreement in the σ values. First, it may be inappropriate to assign statistical segment lengths on the basis of these plots since the plateaus extend to wavevectors as high as 0.8 $Å^{-1}$ even though $k = 1/\sigma \approx 0.16$ is considered to be the upper limit of the intermediate scaling regime. Second, while the exact CSR form (eq 7a) was used for the 50-mer solvation potentials, the strength of these potentials was increased for the 200-mers in order to match the experimental characteristic ratio. This difference in potential strength will alter the short-range interactions and likely change the statistical segment length.

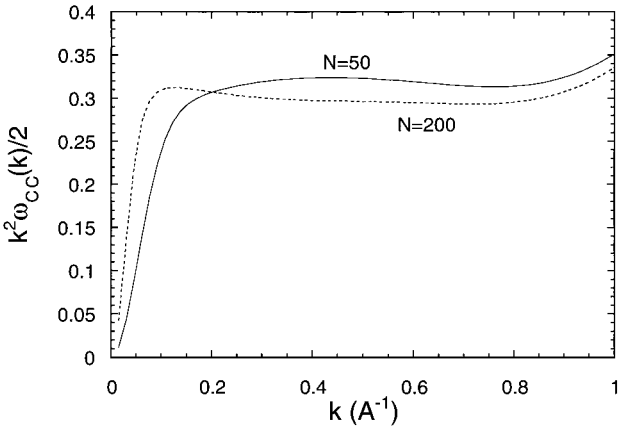

Figure 7. Kratky plot of the intermediate wavevector intramolecular structure between C sites of polyisobutylene. The solid and dashed lines correspond to PIB molecules of length 50 and 200, respectively.

The Kratky plots for pairs AB and BB for all three of the polyolefins are very similar to Figure 6 for the AA correlations in PIB. The AC and BC structure factors are very different from the others. Figure 8 shows this plot for AC pairs in PIB. The trend for BC is nearly identical not only for PIB but the other polyolefins as well. The trend for these pairs resembles a narrower plateau than seen in the CC plots, but the data begin to decrease at higher wavevectors in contrast to all of the other pairs.

The last of the three regions of intramolecular structure to be examined is at high wavevectors. A representative plot is shown for $\omega_{cc}(k)$ for PIB in Figure 9. The data for the two chain lengths show slight differences especially at wavevectors between 1 and 2 $Å^{-1}$, which are just above the intermediate scaling regime. However, since the correlations that remain in this range of k are primarily due to carbon−carbon bond lengths, bond angles, and other sites separated by only a few bonds, this structure in general is chain length independent.

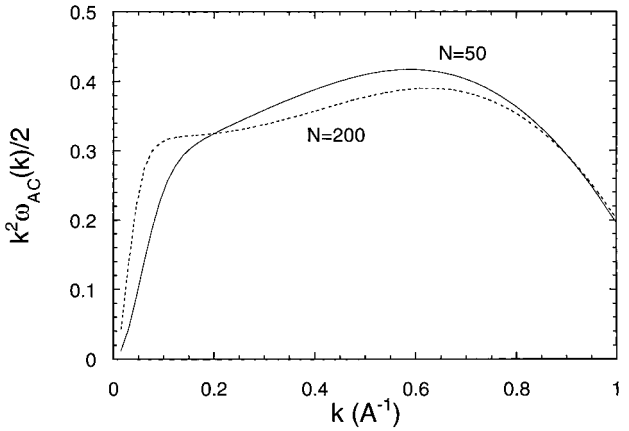

Figure 8. Kratky plot of the intermediate wavevector intramolecular structure between A and C pairs in polyisobutylene. The solid and dashed lines correspond to PIB molecules of length 50 and 200, respectively.

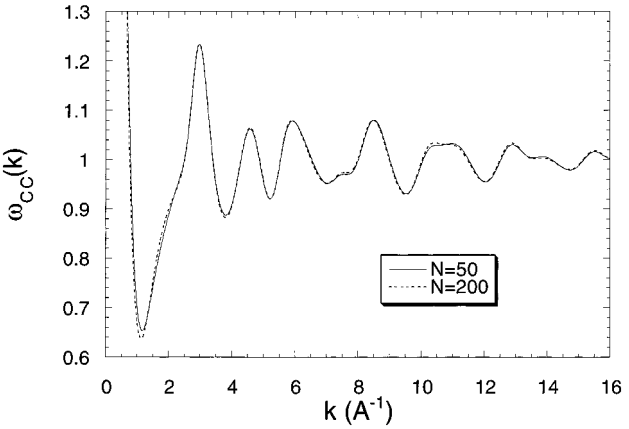

Figure 9. High wavevector intramolecular structure between C sites of PIB. The data for 50-mers (solid line) and 200-mers (dashed line) are very similar.

The chain length dependence of self-consistent intramolecular correlations suggests that approximate structure factors for high molecular weight polymers may be found by first determining the structure of shorter chains and then extrapolating the behavior to high molecular weight. The most significant difference occurs at low wavevectors where the slope of an Ornstein−Zernike plot is proportional to R_g. More studies are necessary to determine the behavior in the intermediate scaling regime for long chains. This work will be the subject of future investigations.

In addition to the molecular weight dependence, comparisons can also be made between structures determined self-consistently and those assuming screened excluded-volume interactions. Figure 10 compares Kratky plots of the CC correlations for 200-mers of PIB. The screened results were generated with a united atom model having fixed bond angles as in past work.[16] Since the rms radii of gyration of these molecules are identical, the structure factors are the same in the very low wavevector Ornstein−Zernike region. However, the height of the plateau region is significantly lower for the self-consistent structure. The inset to Figure 10 compares the structures at high wavevectors. The disagreement between the two approaches in this wavevector regime is primarily due to one model having fixed bond angles while the other model allows these angles to vary.

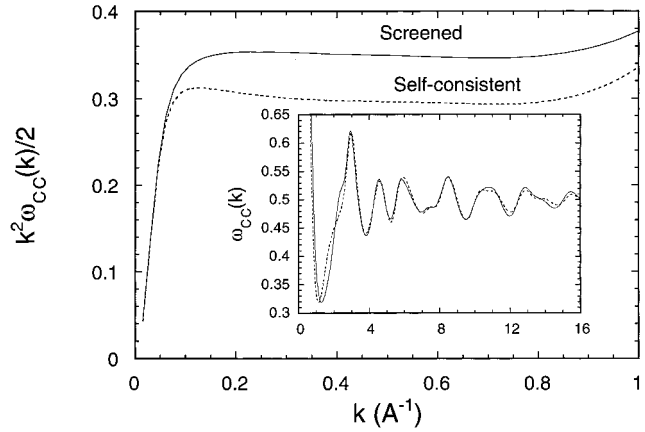

Figure 10. Comparison of intramolecular structure factors determined from self-consistent calculations (dashed line) and screened excluded-volume simulations (solid line). Correlations between C sites for 200-mers of PIB are shown in Kratky format. The inset presents the high wavevector structure in standard format.

On the basis of the difference in height of the intermediate wavevector plateaus, eq 13 suggests that the statistical segment length, σ, is larger for the self-consistent results. Since the screened excluded-volume simulations allow overlaps between sites separated by more than six bonds, these molecules should be more flexible and have a lower σ. However, it is interesting that the same end-to-end distance can be obtained from two molecules with the same number of monomers but different statistical segment lengths. This behavior can be explained best by recognizing that eq 13 and the dependence of end-to-end distance on statistical segment length are based on the assumption that the conformations follow Gaussian statistics. While the screened excluded-volume conformations must be Gaussian in the long chain limit, the self-consistent conformations deviate from this behavior in two ways: (1) the conformations must be self-avoiding, and (2) the additional solvation potential counteracts the tendency toward swollen conformations and favors the alignment of sites into coordination shells. A measure of the deviation of the conformation distribution from Gaussian statistics is provided by the ratio $\langle R^4\rangle/\langle R^2\rangle^2$ of the fourth moment of the end-to-end distance to the second moment squared. The screened excluded-volume simulations indicate this ratio to be 1.64, which agrees closely with $^5/_3$, the value expected for long Gaussian chains. The self-consistent conformations give a ratio of 1.40, which is intermediate between Gaussian chains and rigid rods (ratio = 1.0). Therefore, the self-consistent structure has a significant amount of non-Gaussian character, and analyses based on these statistics may be unreliable.

Although Figure 10 shows that the self-consistent and screened excluded-volume structure factors for CC pairs are not identical, the main differences for all of the pairs appear to be in the magnitude within the intermediate wavevector regime. Given a method to estimate the difference in the magnitude in this wavevector regime, it would be possible to approximate a self-consistent structure through corrections to less computationally demanding screened excluded-volume simulations. However, since the differences in self-consistent structures at various chain lengths are closely linked to measurable properties (i.e., R_g), the extrapolation of these structures to high molecular weight is more likely to

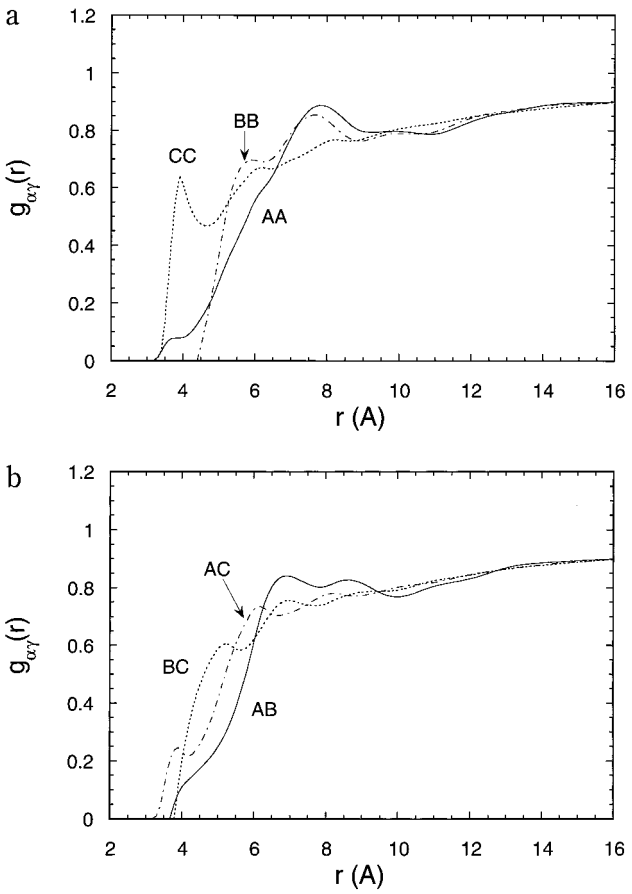

Figure 11. Intermolecular radial distribution functions for PIB: (a) correlations between site of the same type; (b) correlations between unlike pairs of sites.

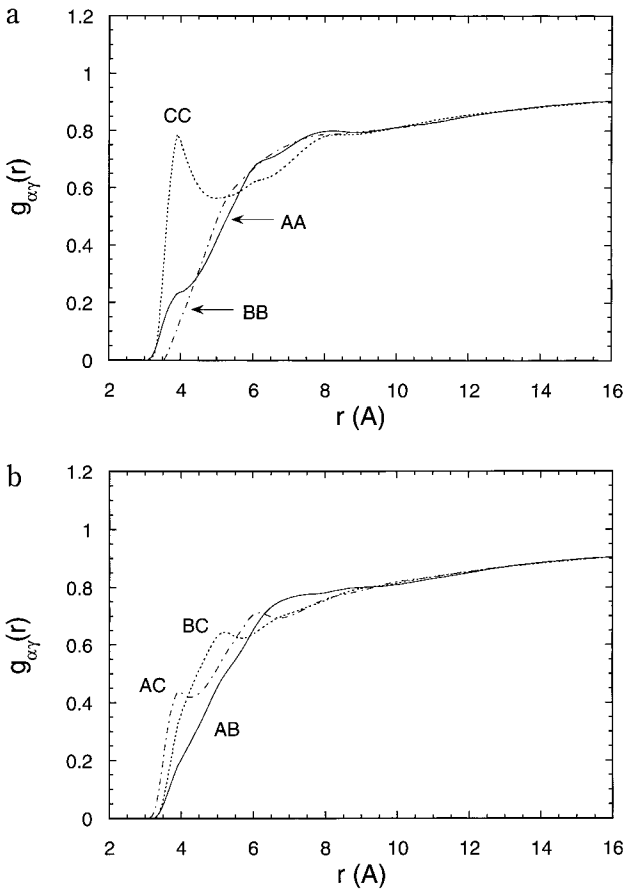

Figure 12. Intermolecular radial distribution functions for isotactic polypropylene: (a) correlations between site of the same type; (b) correlations between unlike pairs of sites.

produce accurate structure factors than corrections to screened excluded-volume simulations.

4.3. Intermolecular Structure. The intermolecular pair correlation functions, $g_{\alpha\gamma}(r)$, and total structure factors, $\hat{S}_{\alpha\gamma}(k)$, are the output of PRISM theory. Since these functions are critical for determining properties such as the miscibility of polymer blends, the ability to quickly solve for these functions at a variety of compositions represents one of the greatest advantages of PRISM. A primary focus of this paper is comparing the structure factors to X-ray scattering experiments. However, we first examine the pair correlation functions in order to understand the differences in the ways that polyolefins pack together.

Figure 11 shows $g(r)$ for PIB chains of 200 monomers. At distances beyond ~12 Å, each of the pair correlations are nearly identical and approach $g(r) = 1$ as r exceeds the separation between the most distant intramolecular sites. This is the universal correlation hole regime whose structure depends only on the radius of gyration but is insensitive to the local monomeric structural details.

On short length scales, it can be seen from Figure 11 that the individual pair correlation functions show nonuniversal behavior. These local packing correlations depend sensitively on the local geometric structure of the monomers. The most prominent feature is a sharp peak in the CC pair function at a distance just above contact. This peak occurs because the C sites are more exposed than either of the backbone sites, and the closest contact between two PIB molecules is likely to be between C sites. A similar but less prominent peak also appears in the AC correlation. All of the pairs show peaks and minima at intermediate distances, suggesting a tendency for the sites to align into ordered solvation shells. Several of the distribution functions demonstrate one of these solvation shells as a peak at approximately 7 Å. The BB pair function shows unusual behavior at distances near contact in which $g(r)$ actually becomes zero at distances greater than the distance of closest approach between two isolated B sites. This behavior is a consequence of the shielding of the B sites caused by the attached methyl groups.

Pair correlation functions for isotactic and syndiotactic polypropylene are shown in Figures 12 and 13. The distribution functions for these stereoisomers are very similar although sPP has a lower first peak for $g_{cc}(r)$. The pair correlations for both forms of polypropylene demonstrate several of the features observed for PIB such as the strong peak in $g_{cc}(r)$ at a distance just below 4 Å. However, the functions tend to merge with one another at a shorter distance (~9 Å) than PIB, and the oscillations at intermediate distances have a smaller amplitude. The small size of these oscillations suggests that polypropylene molecules pack together in a less ordered manner than PIB. As in PIB, $g_{BB}(r)$ approaches zero at distances larger than the site diameter. Since the B site is shielded by a single methyl group in polypropylene, the problems encountered by using the PY closure on a shielded site are reduced.

Figure 14 compares $g_{cc}(r)$ for 200 monomer chains of PIB and iPP. The higher degree of order in PIB packing is not as apparent with the CC pairs, but the two $g(r)$ differ significantly in the peak near contact at ~4 Å. Since PIB has two methyl groups on every monomer,

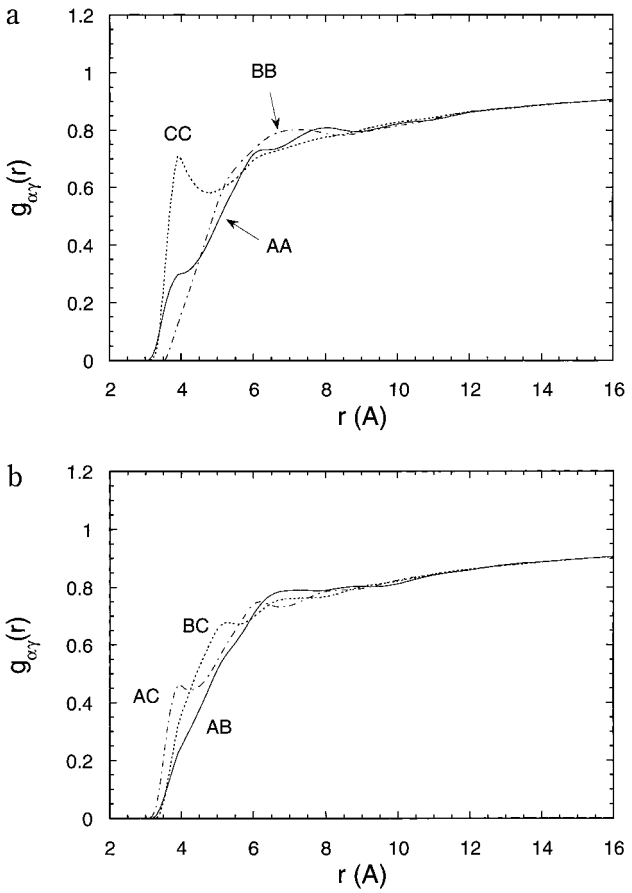

Figure 13. Intermolecular radial distribution functions for syndiotactic polypropylene: (a) correlations between site of the same type; (b) correlations between unlike pairs of sites.

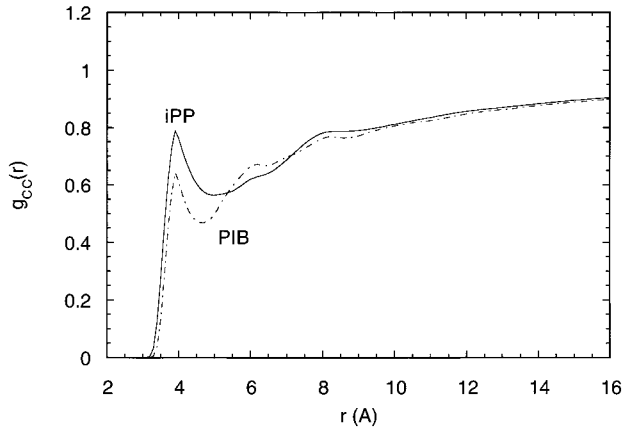

Figure 14. Comparison of the intermolecular pair correlation functions between C sites for isotactic polyproylene (solid line) and polyisobutylene (dot−dashed line).

each C site is partially shielded by the other C site. Therefore, these sites on PIB are unable to have as many intermolecular contacts as iPP, and $g_{cc}(r)$ has a lower value near contact. Even though this peak is smaller for PIB, the C site has even more influence on the properties of PIB since each monomer has two C sites.

Since intermolecular interactions are strongest for short-range correlations, the pair distribution functions demonstrate that the properties of the C site are extremely important. For example, the heat of mixing of one of these polymers with any other molecule will be strongly dependent on the dispersive interaction strength of the C site. Future papers will test the predictions of mixing behavior through calculations of gas solubility in polymers and polymer blend miscibility. To test the predicted melt structure, comparison to wide-angle X-ray scattering experiments is appropriate.

4.4. Comparison to X-ray Scattering Experiments. Details about the wide-angle X-ray scattering experiments and data analysis have been discussed previously.[16,50] The measurements were taken over the range of wave vectors $0.3 \le k \le 16\text{A}^{-1}$. After standard corrections and normalization to the scattering from uncorrelated scattering sites, the experimental structure factor $\hat{S}_{exp}(k)$ was obtained. To emphasize the contributions from local bonded correlations, the structure factor is shown in the form

$$\hat{H}_{exp}(k) = \frac{N_S(\hat{S}_{exp}(k) - \hat{S}_s(k))}{[b_A(k) + b_B(k) + n_C b_C(k)]^2} \qquad (14)$$

where $\hat{S}_s(k) = \sum_m b_m^2(k)$ is the self-scattering contribution, $b_m(k)$ are the scattering contrast factors for the m = A, B, or C sites, and n_c is the number of C sites. The contrast factors were calculated from ref 51. N_s is the number of sites per monomer which normalizes the structure factor to a per monomer basis.

For better computational efficiency the Monte Carlo simulations imposed fixed bond lengths even though a real bond will undergo high-frequency vibrations. The effect of these vibrations on the intramolecular structure functions can be included in an approximate manner through Debye−Waller corrections.[51] Corrections were also added for bond bending vibrations based on the average value of each bond angle obtained from the simulation. Finally, the Debye−Waller factors for all pairs separated by more than two bonds were assumed to be equal and were adjusted to get the best agreement between the modeled structure factor and experiment at high wave vectors. Note that these vibrational corrections only affect the short-range (high wavevector) correlations in the structure factor and should not affect the low wavevector correlations which are dominated by intermolecular packing.

To compare to the experimental scattering, we must combine the individual structure functions from PRISM into a single total scattering function:

$$\hat{S}_{PRISM}(k) = \sum_{mm'} b_m(k)\, b_{m'}(k)\, \hat{S}_{mm'}(k) \qquad (15)$$

After weighting the structure functions by the site X-ray contrast factors, $\hat{S}_{PRISM}(k)$ is normalized through eq 14 and then compared directly to experiment. Figures 15−17 compare these structure factors for PIB, iPP, and sPP, respectively. In each case the PRISM predictions show close agreement with the experimental results. Since long-range correlations in these structure factors diminish quickly as wavevector increases, the behavior of $H(k)$ above $k \approx 3$ Å^{-1} is dominated by short-range intramolecular correlations. The agreement over this range indicates that the bond lengths, angles, and other pairs separated by a few bonds in $\hat{\omega}_{ij}(k)$ are representative of the true polymer. Meanwhile, the first peak in the structure factor is dominated by longer-range intermolecular correlations. Since these correlations are determined by PRISM, the close agreement for this peak demonstrates that the intermolecular packing predicted by the theory is consistent with experiment.

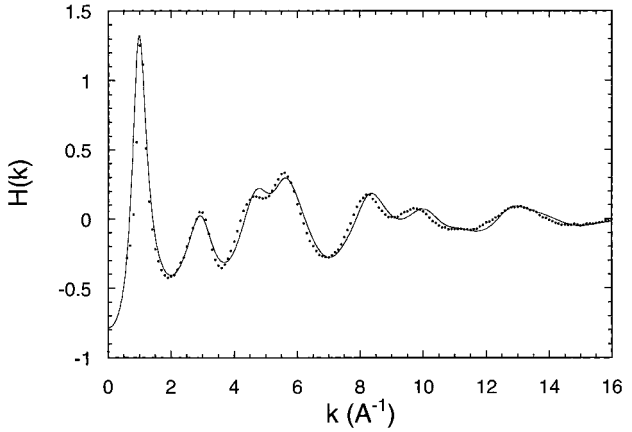

Figure 15. X-ray structure factors for polyisobutylene. The symbols are the experimental data at 25 °C. The solid line is the PRISM prediction.

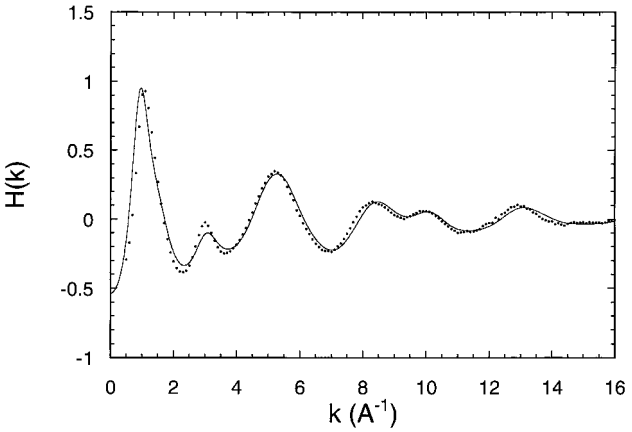

Figure 16. X-ray structure factors for isotactic polypropylene. The symbols are the experimental data at 180 °C. The solid line is the PRISM prediction.

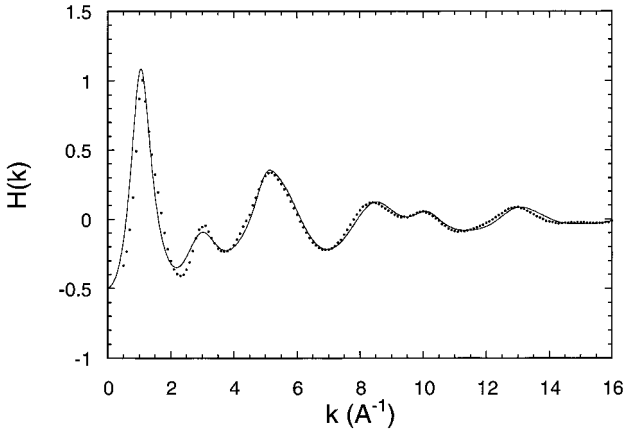

Figure 17. X-ray structure factors for syndiotactic polypropylene. The symbols are the experimental data at 180 °C. The solid line is the PRISM prediction.

Comparison of the X-ray structure factors for the three polymers shows some interesting features. As may be expected, the structure factors of isotactic and syndiotactic polypropylene are very similar. Since the extra methyl branch of PIB provides additional intramolecular correlations, the $k > 3$ Å^{-1} part of the structure factor is somewhat different from the polypropylenes especially in the region 4 Å$^{-1} < k < 6$ Å^{-1}. However, the most distinct difference between the PIB and PP structure is the width of the first peak. This peak is usually observed at $k \approx 2\pi/\Delta r$ where Δr is the spacing between the peaks in $g(r)$.[32] Therefore, a narrow first peak in $H(k)$ as seen in PIB corresponds to well-defined and evenly spaced peaks in $g(r)$ whereas the absence of order in the polypropylene $g(r)$'s does not allow a clear value of Δr to be assigned and results in a broad first peak in $H(k)$. The ability of PIB to pack in an ordered manner allows it to have a higher density than other polyolefins, and this difference in packing is the most likely source of the excellent gas barrier properties of butyl rubber.

Comparisons can also be made between the predicted polypropylene X-ray structures in Figures 16 and 17 and those from previous PRISM studies[16] which assumed screened excluded volume. Although the two routes show almost the same level of agreement with experiment, the self-consistent calculations were obtained without resorting to several approximations that were necessary for the screened excluded-volume case. One of these approximations required an estimate of the volume of intramolecular overlap in order to determine the density at which PRISM will match the occupied volume of the real polymer melts. Due to numerical problems caused by overlaps between three or more sites, recent studies[16] determined the corrected density by matching the zero wavevector structure factor to experimental compressibility data. Not only does this calculation require additional experimental data, but the PRISM prediction of $S(k=0)$ is also affected by using only the repulsive part of the interaction potential in the Percus−Yevick closure. Also, the PRISM stage of the screened excluded-volume calculations has generally used a single hard core diameter (typically $\sigma = 3.90$ Å) for each of the sites. Even for the repulsion between two methyl sites, in which the σ and ϵ parameters are higher than for any of the other sites, the effective hard core size is substantially smaller than 3.90 Å. Therefore, the use of a relatively high hard core diameter likely cancels some of the error created by the other approximations. In contrast, the PRISM step of the self-consistent calculation uses standard united atom parameters,[37,38] and these values matched those employed for the longer-range interactions of the single-chain simulations. Therefore, a consistent set of potentials is used in both stages of the calculation, and since there is no need for experimental compressibility data, the ability to predict the structure of polymers before they have been synthesized is improved. Thus, the additional computational complexity of a self-consistent calculation does not necessarily result in better agreement with experiment, but it does avoid several approximations and the need for experimental data that are necessary whenever screened excluded volume is assumed.

5. Conclusions

This paper has presented atomistically realistic self-consistent PRISM calculations and comparisons to X-ray scattering experiments for isotactic and syndiotactic polypropylene and polyisobutylene. The technique consisted of two stages: (1) a Monte Carlo simulation to determine the structure of a single molecule and (2) a PRISM theory calculation that predicts the structure of the melt and the effect of the rest of the melt on the single chain. A self-consistent solution was obtained after 20−30 iterations through these two stages. This self-consistent procedure has the advantage that one set of potentials should be transferrable from one polymer to the next and that the experimental density can be

used in the PRISM step rather than an overlap-corrected value as used in earlier studies.

The structure factors predicted for each of the polyolefins match closely to data from X-ray scattering experiments. While isotactic and syndiotactic polypropylene have very similar structure factors, they differ significantly from PIB in the width of the lowest wavevector peak. The narrow shape of this peak for PIB indicates that these polymers pack in a highly ordered manner which allows the melts to have a relatively high density. This difference in the degree of order is also apparent in the intermolecular pair correlation functions. The ability to pack in an efficient manner is a primary reason why PIB has much better gas barrier properties than polypropylene melts.

The dependence of the intramolecular structure factors on molecular weight was examined over three different regions of wavevector. The observed trends, such as a simple dependence on R_g at very low wavevectors, suggest that reasonably accurate structure factors for high molecular weight polymers may be determined by extrapolations of the correlation functions for shorter chains. Although Kratky plots for methyl−methyl correlations suggest a well-defined value of the statistical segment length, the overall conformations appear to deviate significantly from Gaussian statistics.

While future studies will compare the structure predicted by self-consistent PRISM theory to many-chain simulations of the same model, the close agreement between the predicted structure factors and X-ray scattering experiments suggests that this PRISM technique is an effective route to the molecular properties of polymers. For realistic models, this technique reduces the problem of simulating a large collection of polymers to the simulation of only a single molecule. Thus, it becomes possible to use efficient Monte Carlo algorithms and to study molecular weights that would otherwise require systems that are too large to simulate in a reasonable amount of computer time. Comparison of PRISM and molecular dynamics studies of a united atom model of polyethylene with 66 CH_2 units suggests that the many-chain simulations require a factor of 20 more computation time than PRISM. This factor is likely to increase further with chain length. Therefore, self-consistent PRISM theory can be a computationally efficient alternative to performing many-chain simulations.

Acknowledgment. The authors thank J. D. McCoy, A. Yethiraj, and K. S. Schweizer for extremely helpful comments and suggestions.

References and Notes

(1) Krishnamoorti, R.; Graessley, W. W.; Fetters, L. J.; Garner, R. T.; Lohse, D. J. *Macromolecules* **1995**, *28*, 1252.
(2) Maranas, J. K.; Mondello, M.; Grest, G. S.; Kumar, S. K.; Debenedetti, P. G.; Graessley, W. W. *Macromolecules* **1998**, *31*, 6991; *Macromolecules* **1998**, *31*, 6998.
(3) Vacatello, M.; Yoon, D. Y. *Macromolecules* **1992**, *25*, 2502.
(4) Pant, P. V. K.; Han, J.; Smith, G. D.; Boyd, R. H. *J. Chem. Phys.* **1993**, *99*, 597. Boyd, R. H.; Pant, P. V. K. *Macromolecules* **1991**, *24*, 6325.
(5) Kumar, S. K.; Vacatello, M.; Yoon, D. Y. *J. Chem. Phys.* **1988**, *89*, 5206.
(6) Kremer, K.; Grest, G. S. In *Monte Carlo and Molecular Dynamics Simulations in Polymer Science*; Binder, K., Ed.; Oxford University Press: New York, 1995.
(7) For recent reviews see: Schweizer, K. S.; Curro, J. G. *Adv. Polym. Sci.* **1994**, *116*, 321. Schweizer, K. S.; Curro, J. G. *Adv. Chem. Phys.* **1997**, *98*, 1.
(8) Schweizer, K. S.; Curro, J. G. *Phys. Rev. Lett.* **1987**, *58*, 246.
(9) Curro, J. G.; Schweizer, K. S. *Macromolecules* **1987**, *20*, 1928.
(10) Curro, J. G.; Schweizer, K. S. *J. Chem. Phys.* **1987**, *87*, 1842.
(11) Curro, J. G.; Schweizer, K. S.; Grest, G. S.; Kremer, K. *J. Chem. Phys.* **1989**, *91*, 1357.
(12) Honnell, K. G.; Curro, J. G.; Schweizer, K. S. *Macromolecules* **1990**, *23*, 3496.
(13) Koyama, R. *J. Phys. Soc. Jpn.* **1973**, *34*, 1029.
(14) Lal, M. *Mol. Phys.* **1965**, *17*, 57.
(15) Flory, P. J. *J. Chem. Phys.* **1949**, *17*, 203.
(16) Curro, J. G.; Weinhold, J. D.; Rajasekaran, J. J.; Habenschuss, A.; Londono, J. D.; Honeycutt, J. D. *Macromolecules* **1997**, *30*, 6264.
(17) Schweizer, K. S.; Curro, J. G. *Macromolecules* **1988**, *21*, 3070.
(18) Chandler, D.; Andersen, H. C. *J. Chem. Phys.* **1972**, *57*, 1930.
(19) Chandler, D. In *Studies in Statistical Mechanics VIII*; Montroll, E. W., Lebowitz, J. L., Eds.; North-Holland: Amsterdam, 1982.
(20) Chandler, D.; Pratt, L. R. *J. Chem. Phys.* **1976**, *65*, 2925. Pratt, L. R.; Chandler, D. *J. Chem. Phys.* **1977**, *66*, 147.
(21) Pettitt, B. M.; Karplus, M.; Rossky, P. J. *J. Phys. Chem.* **1986**, *90*, 6335. Ichiye, T.; Chandler, D. *J. Phys. Chem.* **1988**, *92*, 5257.
(22) Schweizer, K. S.; Honnell, K. G.; Curro, J. G. *J. Chem. Phys.* **1992**, *96*, 3211.
(23) Yethiraj, A.; Schweizer, K. S. *J. Chem. Phys.* **1992**, *97*, 1455.
(24) Melenkevitz, J.; Curro, J. G.; Schweizer, K. S. *J. Chem. Phys.* **1993**, *99*, 5571.
(25) Grayce, C. J.; Yethiraj, A.; Schweizer, K. S. *J. Chem. Phys.* **1994**, *100*, 6857.
(26) Melenkevitz, J.; Schweizer, K. S.; Curro, J. G. *Macromolecules* **1993**, *26*, 6190.
(27) Grayce, C. J.; Schweizer, K. S. *Macromolecules* **1995**, *28*, 7461.
(28) David, E. F.; Schweizer, K. S. *J. Chem. Soc., Faraday Trans.* **1995**, *91*, 2411.
(29) Khalatur, P. G.; Khokhlov, A. R. *Mol. Phys.* **1988**, *93*, 555.
(30) Gromov, D. G.; de Pablo, J. J. *J. Chem. Phys.* **1995**, *103*, 8247.
(31) Curro, J. G. *Macromolecules* **1994**, *27*, 4665.
(32) Hansen, J. P.; McDonald, I. R. In *Theory of Simple Liquids*, 2nd ed.; Academic: New York, 1986.
(33) Ballard, D. G.; Schelton, J.; Wignall, G. D. *Eur. Polym. J.* **1973**, *9*, 965. Cotton, J. P.; Decker, D.; Benoit, H.; Farnoux, B.; Higgins, J.; Jannick, G.; Ober, R.; Picot, C.; des Cloizeaux, J. *Macromolecules* **1974**, *7*, 863.
(34) Curro, J. G. *J. Chem. Phys.* **1974**, *61*, 1203. Curro, J. G. *Macromolecules* **1979**, *12*, 463.
(35) Chandler, D.; Singh, Y.; Richardson, D. M. *J. Chem. Phys.* **1984**, *81*, 1975. Nichols, A. L.; Chandler, D.; Singh, Y.; Richardson, D. M. *J. Chem. Phys.* **1984**, *81*, 5109. Laria, D.; Wu, D.; Chandler, D. *J. Chem. Phys.* **1991**, *95*, 4444.
(36) Grayce, C. J.; Schweizer, K. S. *J. Chem. Phys.* **1994**, *100*, 6846.
(37) Siepmann, J. I.; Martin, M. G.; Mundy, C. J.; Klein, M. L. *Mol. Phys.* **1997**, *90*, 687.
(38) Jorgensen, W. L.; Madura, J. D.; Swenson, C. J. *J. Am. Chem. Soc.* **1984**, *106*, 6638.
(39) McCoy, J. D.; Curro, J. G., submitted to *J. Chem. Phys.*
(40) Metropolis, N.; Rosenbluth, A. W.; Rosenbluth, M. N.; Teller, A. H.; Teller, A. *J. Chem. Phys.* **1953**, *21*, 1087.
(41) Walsh, D. J.; Graessley, W. W.; Datta, S.; Lohse, D. J.; Fetters, L. J. *Macromolecules* **1992**, *25*, 5236.
(42) Zoller, P. *J. Appl. Polym. Sci.* **1979**, *23*, 1057.
(43) Hsu, C. S.; Chandler, D.; Lowden, L. *J. Chem. Phys.* **1976**, *14*, 213. Cummings, P. T.; Gray, C. J.; Sullivan, D. E. *J. Phys. A* **1981**, *14*, 1483.
(44) Yethiraj, A., unpublished results.
(45) Hayashi, H.; Flory, P. J.; Wignall, G. D. *Macromolecules* **1983**, *16*, 1328.
(46) Grayce, C. J. *J. Chem. Phys.* **1997**, *106*, 5171.
(47) Guinier, A. *Ann. Phys.* **1939**, *12*, 161.
(48) Doi, M.; Edwards, S. F. *Theory of Polymer Dynamics*; Oxford Press: Oxford, 1986.
(49) McCoy, J. D.; Honnell, K. G.; Curro, J. G.; Schweizer, K. S.; Honeycutt, J. D. *Macromolecules* **1992**, *25*, 4905.
(50) Londono, J. D.; Habenschuss, A.; Curro, J. G.; Rajasekaran, J. J. *J. Polym. Sci., B: Polym. Phys.* **1996**, *34*, 3055.
(51) Narten, A. *J. Chem. Phys.* **1979**, *70*, 299.
(52) Honnell, K. G.; McCoy, J. D.; Curro, J. G.; Schweizer, K. S.; Narten, A. H.; Habenschuss, A. *J. Chem. Phys.* **1991**, *94*, 4659.
(53) Narten, A. H.; Habenschuss, A.; Honnell, K. G.; McCoy, J. D.; Curro, J. G.; Schweizer, K. S. *J. Chem. Soc., Faraday Trans.* **1992,** *88*, 1791.

MA990150Y